PCCP

Accepted Manuscript

ROYAL SOCIETY OF CHEMISTRY

www.rsc.org/pccp

Electrical tuning of spin current in a boron nitride nanotube quantum dot

Kamal B Dhungana[1] and Ranjit Pati*[1]

[1]*Department of Physics, Michigan Technological University, Houghton MI 49931, USA*

Abstract

Controlling spin current and magnetic exchange coupling by electric field and achieving high spin injection efficiency at the same time in a nanostructure coupled to ferromagnetic electrodes have been the outstanding challenges in nanoscale spintronics. A relentless quest is on to find new low-dimensional materials with tunable spin dependent properties to address these challenges. Herein, we predict, from first-principles, the transverse-electric-field induced switching in the sign of exchange coupling and tunnel magneto-resistance in a boron nitride nanotube quantum dot attached to ferromagnetic nickel contacts. An orbital dependent density functional theory in conjunction with a single particle Green's function approach is used to study the spin dependent current. The origin of switching is attributed to the electric field induced modification of magnetic exchange interaction at the interface caused by the Stark effect. In addition, spin injection efficiency is found to vary from 61% to 89% depending upon the magnetic configurations at the electrodes. These novel findings are expected to open up a new pathway toward the application of boron nitride nanotube quantum dot in next generation nanoscale spintronics.

* e-mail:patir@mtu.edu

I. Introduction

Spintronics, which relies on the spin state of the electron to store, transport, and process information, has been the subject of intense research since the discovery of giant magneto-resistance.[1] With the revolutionary progress in nanotechnology in recent years enabling the manipulation of electron spins in nanoscale tunnel junctions,[2–9] it has crossed the boundary of conventional, all metallic, solid state multi-layered structures[10–12] to reach a new frontier, where nano-structures are being used as controlled spin-carriers. When a quantum-confined nanostructure (QCNS) having a non-magnetic character is used as a tunnel barrier between two magnetic electrodes, it offers new opportunities for the spin manipulation via external electric field — *an important prerequisite for nanoscale spintronics*;[13–15] the QCNS in contact with a ferromagnetic lead loses its non-magnetic property due to the magnetic proximity effect and becomes spin-polarized.[16,17] The external electric field then not only modulates the shape of the spin orbital[14] and position of the discrete spin-polarized eigen-channels of the QCNS due to the Stark effect, but also it modifies the electronic and magnetic structure at the interface,[9,13,15,18–20] which plays a dominant role in dictating the spin current behavior of the device.

For example, using molecular quantum dot, researchers have already demonstrated giant magnetoresistance effect in molecular tunnel (MT) devices.[3,6,7] However, the strong sensitivity of magnetoresistance to the junction structure[21] and the difficulty in achieving atomic level controls at the interface make the implementation of the MT device an arduous task. Other promising nano-structures being investigated as spin-carriers are carbon nanotube quantum dots (CNTQD) coupled to ferromagnetic electrodes.[4,5,22] The gate field induced switching of the exchange field has already been established in this system.[4] In addition, the sign modulations of tunnel magnetoresistance (TMR) in both two and three terminal CNTQD-magnetic junctions have been reported.[5,23] But the difficulty in separating the metallic CNT from the semiconducting one poses a significant hurdle toward their practical applications in spintronics. On the other hand, a robust semiconducting boron nitride nanotube (BNT),[24,25] which is structurally similar to CNT, would be an ideal tunnel barrier for the spin transport because its electronic property is independent of its chirality. BNT is also found to exhibit a giant response to the transverse electric field[26] due to strong Stark effect arising from the ionic nature of BN bonds — *offering new opportunities to control spin current via electric field.* However, up until now, no efforts have been made to understand the spin current in such a device.

Here, we use a boron nitride nanotube quantum dot (BNTQD) as a tunnel barrier between two ferromagnetic nickel electrodes to probe the electric field manipulation of spin current. Our first-principles investigation reveals transverse electric field (ε_g) induced switching in the sign of exchange coupling ($\mathbf{J}$) and tunnel magneto resistance together with

a very high spin injection efficiency. The precise role of BNTQD/Ni interface on switching the sign of **J** and TMR is identified. In addition, we have observed an intriguing bias dependent switching in spin-polarized current with a robust negative differential resistance (NDR) feature at a higher ε_g. The origin of this novel switching property is attributed to the strong field-induced modification of the spin orbitals due to the Stark effect.

The rest of the paper is organized as follows. In the section II, we present briefly the computational procedure. Results and discussions are described in the section III followed by a brief conclusion in the section IV.

II. Computational Method

The spin-up and the spin-down components in the presence of ε_g are calculated within the multichannel Landauer-Büttiker formalism: $I^{\sigma}_{sd} = \frac{e}{h}\int_{\mu_1}^{\mu_2} T^{\sigma}(E, V_{sd}, \varepsilon_g)\times[f(E,\mu_2) - f(E,\mu_1)]\times dE$. $T^{\sigma}(E, V_{sd}, \varepsilon_g)$ is the transmission function obtained from the bias dependent spin-polarized Green's function, which is calculated as: $G^{\sigma}(E, V_{sd}, \varepsilon_g) = [E \times S_{QD} - H^{\sigma}_{QD}(V_{sd}, \varepsilon_g) - \Sigma^{\sigma}_{l}(V_{sd}, \varepsilon_g) - \Sigma^{\sigma}_{r}(V_{sd}, \varepsilon_g)]^{-1}$. $\mu_{1,2}$ are the electro-chemical potentials at the leads, which are determined self-consistently (see Ref. 21 for details). $H_{QD}(V_{sd}, \varepsilon_g)$ is the bias dependent Kohn-Sham Hamiltonian for the BNTQD; $\Sigma^{\sigma}_{l,r}(V_{sd}, \varepsilon_g)$ are the bias dependent spin-polarized self-energy functions, which permit the BNTQD to exchange its spin-polarized electrons and energy with the semi-infinite electrodes. We have considered a chemically bonded junction where the ground state based DFT has been found to be a good approximation.[27–32] The interfacial distance between BNTQD and nickel surface is 1.9 Å, which is obtained by minimizing the repulsive interaction within the spin unrestricted density functional theory. The energy versus interface distance curve is found to be parabolic around 1.9 Å that further justifies the use of ground state based DFT in our calculations. An orbital dependent B3LYP hybrid functional for exchange-correlation and an all-electron 6-311g* Gaussian basis set[33] is used to describe the atoms in the device. A true dynamically corrected spin-polarized exchange correlation potential[34,35] would better represent the transport properties; however, it is difficult to implement in such a system. It should be noted that the use of all electron basis set leads to a spin-polarized Hamiltonian matrix of the active scattering region with a dimension of 1572 × 1572 for each applied bias point. An energy grid of 0.001 eV is used for integration of the transmission. The real space approach adopted here allows us to include the most crucial electronic and magnetic structure details of the BNTQD junction from the first-principles. The modification in the electronic and magnetic structure of the device due to the transverse electric field (ε_g) is incorporated through the inclusion of a dipole interaction term ($\vec{\varepsilon_g}.\sum_i \vec{r}(i)$) in the Kohn-Sham Hamiltonian as a perturbation; the strength of the dipole interaction is much weaker compared to the electronic interaction. Since the perturbed dipole interaction term contains only single particle interactions, we add it to the core Hamiltonian during the self-consistent electronic structure calculation

to include both the first and higher order Stark effects.

III. Results and Discussion

First, we consider a prototypical BNTQD-magnetic tunnel junction as shown in Fig. 1. For a practical reason, an optimized (6,0) BNT of length 12.3 Å is sandwiched between two Ni (111) electrodes to build the open device structure. It should be noted that tunnel junction with CNTQD channel of diameter of $\sim$ 1 nm has been fabricated.[8] Furthermore, gate field induced amplification in a molecular transistor with channel length as small as ours' ($\sim$ 1 nm) has been demonstrated.[36] Since the electrons in the BNT considered here are strongly confined in all three dimensions, and there is a lattice mismatch between BNT and Ni at the interface, we term it as a BNTQD. Then, we recourse to a bias dependent, single particle many-body Green's function approach[18,37–39] to obtain the spin dependent current in the BNTQD tunnel device for the parallel spin configuration (PC) and the anti-parallel spin configuration (APC) between the electrodes. Unlike our early work,[40] here the bias effect is included self-consistently.[21] It is important to note that the self-consistent inclusion of bias allows us to create an imbalance in carrier concentration at the leads; on one lead there is a charge surplus and at the other lead there is a charge depletion resulting to residual resistivity dipoles.[38] This is reflected in the bias dependent planar average electrostatic potential profiles for the PC and APC (Fig. 2). Both the profiles show an almost linear drop in the potential across the junction with constant potentials at the leads. The magnitude of the potential drops at two leads for both PC and APC are different, confirming the asymmetric nature of the BNTQD-Ni interfaces at the electronic level.

Spin polarized current. Since the spin coherence length is expected to be longer than the length of the BNTQD channel considered here, we have adopted a coherent spin conserved tunneling approach[18,21,40–44] where the total current is obtained simply by adding the spin-up and the spin-down currents. The results for the total spin-polarized current as a function of ε_g for the PC and the APC are presented in Figs. 1a and 1b, respectively. The lead is assumed to have a single magnetic domain as shown in the inset of Figs. 1a and 1b. It is noteworthy to mention that in both cases the spin-down states are found to contribute significantly to the total current (see Supporting Information). In the absence of ε_g, the current for the PC (I_{PC}) is found to be higher than the current for the APC (I_{APC}). A steady increase in current is noted for the bias up to $\sim$0.5 V beyond which a non-linear feature in the current is observed for both PC and APC. Remarkably, within the linear current regime, with the increase of ε_g, the I_{PC} is found to decrease in contrast to the increase in I_{APC}. A closer inspection shows a much stronger response to ε_g in the APC compared to that in the PC. For example, at a small bias of 0.2 V, there is a 16% decrease in the I_{PC} compared to an increase of 221% in the I_{APC} when ε_g increases from 0 to 2.04 V/Å. For a higher ε_g, the total currents for both PC and APC

rise initially to reach peak values with the increase of V_{sd} and then drop to valley points with the subsequent increase in V_{sd} before increasing again, revealing clear NDR features. For ε_g = 2.04 V/Å, the peak to valley current ratio (I_p/I_v) in the APC is found to be 1.7; for PC the I_p/I_v is 1.4.

Tunnel magnetoresistance. To quantify this surprisingly contrasting response between the PC and the APC to ε_g, we have calculated the TMR as $(I_{PC}-I_{APC})/I_{APC}$. Fig. 3 summarizes the bias dependent TMR data for $\varepsilon_g = 0.00$ V/Å and 2.04 V/Å. In the absence of the transverse electric field, the signs of TMR values are found to be positive for all the bias points considered here. In contrast, for ε_g = 2.04 V/Å, the signs of TMR values are found to be negative. To elucidate this unique transverse electric field dependent TMR result, we have calculated the TMR as a function of ε_g at a small bias of 0.2 V (Fig. 1c). A significant variation in TMR from +23% to -67% with the switching of sign at a critical electric field ($\sim$ 0.8 V/Å) is noted. We have also performed spin-polarized current calculation using a (7,0) BNTQD channel of same length with the same interface distance to check whether the switching feature in TMR observed here persists for other diameters. Indeed, we have found a similar switching feature in TMR as observed for (6,0) BNTQD (See Supporting Information), which confirms the general nature of our observations irrespective of the diameter of the tube. It should be noted that a significant diameter dependent band-gap modulation with ε_g has been reported in pristine BNT.[45,46] The band-gap modulation has been shown to increase with the tube diameter[45,46] and is found to be independent of chirality. This clearly suggests that a smaller critical field (ε_g^c) than that found in our calculation would be suffice to switch the TMR in a BNTQD junction with larger diameter. In addition, the same order of transverse electric field as predicted here has been applied experimentally on BNT of diameter 16.3 $\pm$ 6 Å to observe giant Stark effect,[26] which implies that our predicted critical field for switching TMR would be accessible to the experiment.[47,48] It is also worthwhile to note that a similar gate field dependent switching in the sign of TMR has been observed at low temperature in a CNTQD-magnetic tunnel junction device.[5]

Magnetic exchange coupling. To understand the origin of switching in the sign of TMR, the magnetic exchange coupling, $\mathbf{J} = E_{PC} - E_{APC}$, is calculated as a function of ε_g (Fig. 1d). E_{PC} and E_{APC} are total energies for the PC and the APC respectively in the extended system. At zero ε_g, **J** is found to be positive with the APC being the more stable configuration. When we increase ε_g from 0 to 2.04 V/Å, the value of **J** is found to decrease toward a negative value with the switching of sign at ε_g of $\sim$ 0.8 V/Å. A strong correlation is found between the variation of **J** and TMR; the switching of **J** is found at a slightly higher ε_g than TMR. This can be understood from the fact that **J** calculation does not consider the imaginary part of the Hamiltonian as incorporated in TMR calculation for the open device. To gain deeper insights into the cause of sign reversal in **J**, we examine the spin profile of the device as a function of

ε_g. Due to strong exchange interactions between the electrons at the interface, the non-magnetic BNTQD becomes spin polarized and the atoms that are in close proximity to Ni gain substantial magnetic property;[16,17] the interface now acts as a spin-interface.[18,19] Since we have B atoms at the one interface and N atoms at the other, there is an asymmetric spin profile at the interfacial atoms. For example, in the case of APC, the average magnetic moment per atom ($\bar{\mu}$) in the nitrogen layer at the close vicinity of Ni lead ($\sim$ 1.3 μ_B per atom) changes from - 0.12 μ_B to -0.07 μ_B when we increase ε_g from 0 to 2.04 V/Å; in the case of boron-nickel interface layer, $\bar{\mu}$ for boron changes from -0.01 μ_B to -0.03 μ_B. For PC, $\bar{\mu}$ in the boron layer at the interface decreases from 0.16 μ_B to 0.13 μ_B by changing ε_g from 0 to 2.04 V/Å; only a small change from 0.47 μ_B to 0.48 μ_B is noted for the $\bar{\mu}$ in the nitrogen layer at the interface. This spin profile at the interface is shown schematically in the inset of Fig. 1d. For $\varepsilon_g < \varepsilon_g^c$, the strong negative exchange interaction between Ni and N at the interface for the APC (favored by the Hund's rule) explains the stability of the anti-parallel configuration over the PC. For $\varepsilon_g > \varepsilon_g^c$, there is a substantial decrease in the magnetic moment of the N at the interface for the APC resulting in a lower negative exchange interaction at the Ni/N spin-interface; at the same time, the magnetic moment of the B at the other interface increases leading to a stronger positive exchange interaction at the Ni/B spin-interface. Conversely, for $\varepsilon_g > \varepsilon_g^c$, a substantial decrease in the magnetic moment at the B for the PC leads to a weaker positive exchange interaction at Ni/B spin-interface. This makes the PC more stable than the APC for $\varepsilon_g > \varepsilon_g^c$. Thus, unambiguously, we confirm that the electric field manipulation of spin-interface is the main cause for switching of **J** and TMR. Now the question arises: What is the mechanism that causes the change in spin profile at the interface between PC and APC ? To answer this, we calculate electric dipole moment α^j and polarizability β^{jk} for PC and APC (shown in the Table I). Since the y-components of dipole moment and polarizability for PC and APC are distinct, each spin configuration responds uniquely to the transverse electric field due to Stark effect.[14] This, in fact, results in an energy cross over and switching of **J**. Next, we turn our focus to another important factor, the spin injection co-efficient, η, which dictates the spin injection efficiency from Ni electrode to BNTQD. It should be noted that spin injection into a semiconductor from a ferromagnetic contact can be measured using spin-resolved two-photon photoemission technique.[49] We have calculated the bias dependent η as:[18] $\eta = (I_{up} - I_{down})/(I_{up} + I_{down})$; I_{up} and I_{down} refer to the spin-up and spin-down components of the current, respectively. For PC, the maximum and minimum spin injection factors (η_{max} and η_{min}) are found to be -0.89 and -0.81, respectively (Fig. 4a). In APC, η_{max} and η_{min} are found to be -0.74 and -0.61, respectively (Fig. 4b). These high values of η suggest that the Ni/BNTQD spin-interface acts as an natural spin-selective tunnel barrier for spin injection.

Spin dependent transmission. To further our understanding of the observed ε_g dependent spin current behavior

in PC and APC, we have analyzed the $T^{\sigma}(E, V_{sd}, \varepsilon_g)$. For brevity, the results for T^{σ} at two representative $\varepsilon_g s$ (0 and 2.04 V/Å) are summarized in Figs. 5a and 5b. In both PC and APC, we find a substantially higher contribution to the transmission from the spin-down states, which explains the higher observed spin-down current (see Supporting Information). A significant broadening occurs in the spin-down case for both PC and APC, which can be inferred from the spilling of Ni spin-down density of states (SD-DOS) into the BNTQD due to the strong coupling at the interface and a much higher SD-DOS of the Ni-lead at the Fermi energy. The asymmetry in T^{σ} between spin-up and spin-down states for the APC is expected due to intrinsic structural asymmetry at the interface and the bias induced electronic asymmetry. Transmission data show a much weaker response to ε_g in the case of PC as compared to the APC, which is also reflected in their respective total spin-polarized currents. A closer inspection of Figs. 5a and 5b reveals that the height of the transmission feature near the Fermi energy decreases for the PC with the increase of ε_g (Fig. 5a). In contrast, a substantial increase in the height of the transmission feature is observed for the APC near the Fermi energy with increasing ε_g (Fig. 5b). This clearly explains the observed decrease in current for the PC compared to an increase in current for the APC at a smaller bias with increasing ε_g. In the absence of ε_g, the transmission height for the PC in the vicinity of the Fermi energy is higher than that in APC resulting a higher I_{PC} than I_{APC} (Figs. 1a and 1b).

Nonlinear spin-polarized current. Now the question arises: What is the cause for the strong non-linear NDR behavior in the spin-polarized current at a higher ε_g? To answer this subtle question, we have looked at the T^{σ} at ε_g = 2.04 V/Å for both the PC and the APC. Since the APC shows a much stronger non-liner response at a higher ε_g, we have summarized the results for only the APC (Fig. 6a); only four bias points are considered. The transmission height decreases within the chemical potential window (CPW) for the spin-down states as V_{sd} increases from 0.35 V to 0.72 V. However, since the width of the CPW is much higher for V_{sd} = 0.72 V and the current is dictated by the area under the transmission curve within the CPW, we observe a higher current at V_{sd} = 0.72 V. When we increase the bias further to V_{sd} = 1.51 V, in spite of the increase in CPW width, we see a substantial drop in the height of the transmission within CPW resulting in a significant drop in current leading to a NDR feature. A similar drop in transmission with increase in bias leading to NDR feature has been observed in molecular junction.[50] It should be pointed out that V_{sd} = 0.72 V and 1.51 V correspond to the peak-current and valley-current position respectively for the APC. When we increase V_{sd} to 1.92 V, the spin-up states start contributing significantly within the CPW leading to an increase in total current. The next question is: Why do we see a significant drop in transmission with the increase in V_{sd}? We examine the bias dependent spin orbital for the APC and its response to ε_g to answer this inquiry.

One of the frontier spin-down orbitals (i.e the highest occupied orbital of the active scattering region, HOMO) that contributes to the transmission within the CPW is presented in the inset of Fig. 6a. A dramatic transformation in the shape of the spin orbital is noticeable as V_{sd} changes from 0.35 V to 1.51 V. For $V_{sd} = 0.35$ V, the electron (spin-down) cloud is distributed at both the interfaces despite some asymmetry in distribution between the two interfaces. With the increase of V_{sd}, the asymmetry in electron density distribution between two interfaces increases; at $V_{sd} = 1.51$ V (valley point), due to the strong field induced orbital mixing, the electron cloud is distributed only at the Ni/B interface resulting in a smaller T^{σ}, and hence I^{σ}.

Stark effect. To understand the non-linear response at higher ε_g in greater detail, we then examine the Stark shift for both PC and APC for the extended system (Fig. 6b). The Stark shift is calculated as: $\delta E^n = \epsilon_g^n(V_{sd}) - \epsilon_g(V_{sd} = 0)$, where n corresponds to different participating spin orbitals and ϵ_g is the energy of the spin orbital in the presence of ε_g and V_{sd}. H0 — the energy of the spin-down HOMO at equilibrium — is considered as the reference energy, $\epsilon_g(V_{sd} = 0)$. Since spin-down states dictate the behavior of the current, we have presented the results only for the spin-down states at $\varepsilon_g = 0$ and 2.04 V/Å. A strong non-linear Stark shift ($\sum_j \alpha^j \varepsilon_g^j + \frac{1}{2}\sum_{j,k} \beta^{jk}\varepsilon_g^j\varepsilon_g^k + ...$) for the frontier orbitals at a higher bias is noticeable at $\varepsilon_g = 2.04$ V/Å. Each spin orbital responds differently to ε_g as each orbital has a unique electron density distribution with distinctive dipole moment and polarizability. APC is found to exhibit a much stronger response to the transverse electric field (energy level spacing between H0 and H1 decreases significantly) than the PC. This can also be inferred from the calculated dipole moment and polarizability (Table I). In the case of the APC, α^y and β^{zy} (components along the transverse field direction) are much stronger than that in PC.

IV. Conclusions

We have demonstrated electrical manipulation of quantum spin state of the electron in a BNTQD-magnetic tunnel junction device to show switching in the sign of exchange coupling and tunnel magnetoresistance. Most importantly, the switching feature in tunnel magnetoresistance observed here is found to be independent of the diameter of the BNTQD channel, confirming the general nature of our prediction. Electric field induced Stark effect causing a change in magnetic exchange interaction at the interface is found to be the main mechanism behind the switching in sign. In addition, we have observed a very high spin injection efficiency from nickel electrode to BNTQD. We expect the magnitude of the critical electric field for switching the sign of tunnel magnetoresistance to decrease with the increase in diameter of the BNTQD as revealed from the band-gap modulation study in pristine BNT. Since the predicted external electric field for switching the sign of tunnel magnetoresitance is within the range accessible to the

experiment, we expect our findings would open up new initiatives for the application of the BNTQD tunnel device in next generation spin based nano-scale electronics.

Acknowledgements

This work is supported by NSF through Grant No. 1249504. The results reported here were obtained using RAMA and Superior − the high performance computing cluster of the Michigan Technological University.

Corresponding Author

*E-mail: patir@mtu.edu.

Notes

The authors declare no competing financial interest.

---

[1] A. Fert, *Rev. Mod. Phys.*, 2008, **80**, 1517-1530.

[2] M. Ouyang and D. D. Awschalom, *Science*, 2003, **301**, 1074-1078.

[3] S. Schmaus et al., *Nat. Nanotechnol.*, 2001, **6**, 185-189.

[4] J. R. Hauptmann, J. Paaske and P. E. Lindelof, *Nature. Phys.*, 2008, **4**, 373-376.

[5] S. Sahoo *et al.*, *Nature. Phys.*, 2005, **1**, 99-102.

[6] R. Yamada, M. Noguchi and H. Tada, *J. Appl. Phys.*, 2013, **113**, 144313-7.

[7] K. Horiguchi, T. Sagisaka, S. Kurokawa and A. Sakaia, *J. Appl. Phys.*, 2013, **113**, 144313-7.

[8] M. Urdampilleta, S. Klyatskaya, J-P Cleuziou and M. Ruben, *Nature Mater.*, 2011, **10**, 502-506.

[9] C. Barraud *et al.*, *Nature Phys.*, 2010, **6**, 615-620.

[10] M. N. Baibich *et al.*, *Phys. Rev. Lett.*, 1988, **61**, 2472-2475.

[11] G. Binasch, P. Grunberg, F. Saurenbach and W. Zinn, *Phys. Rev. B*, 1989, **39**, 4828-4830.

[12] S. S. P. Parkin, N. More and K. P. Roche, *Phys. Rev. Lett.*, 1990, **64**, 2304-2307.

[13] V. A. Dediu, L. Hueso, I. Bergenti and C. Taliani, *Nature Mat.*, 2009, **8**, 707-716.

[14] W. Y. Kim and K.S. Kim, *Acc. Chem. Res.*, 2010, **43**, 111-120.

[15] S. Sanvito, *Chem. Soc. Rev.*, 2011, **40**, 3336-3355.

[16] D, Liu, Y. Hu, H. Guo and X. F. Han, *Phys. Rev. B*, 2008, **78**, 193307-193310.

[17] N. Atodiresei *et al.*, *Phys. Rev. Lett.*, 2010, **105**, 066601-4.

[18] D. Waldron, P. Haney, B. Larade, A. MacDonald and H. Guo, *Phys. Rev. Lett.*, 2006, **96**, 166804-4.

[19] S. Sanvito, *Nature Phys.*, 2010, **6**, 562-564.

[20] P. Ruden, *Nat. Mater.*, 2011, **10**, 8-9.

[21] S. Mandal and R. Pati, *ACS Nano.*, 2012, **6**, 3580-3588.

[22] K. Tsukagoshi, B. W. Alphenaar and H. Ago, *Nature(London)*, 1999, **401**, 572-574.

[23] B. Wang, Y. Zhu, W. Ren, J. Wang and H. Guo, *Phys. Rev. B*, 2007, **75**, 235415.

[24] N. G. Chopra *et al.*, *Science*, 1995, **269**, 966-967.

[25] D. Golberg *et al.*, *ACS Nano.*, 2010, **4**, 2979-2993.

[26] M. Ishigami, J. D. Sau, S. Aloni, M. L. Cohen and A. Zettl, *Phys. Rev. Lett.*, 2005, **94**, 056804.

[27] J. Taylor, H. Guo and J. Wang, *Phys. Rev. B*, 2001, **63**, 245407-13.

[28] M. Di Ventra, S. T. Pantelides, and N.D. Lang, *Phys. Rev. Lett.*, 2000, **84**, 979982.

[29] M. Brandbyge, J. L. Mozos, P. Ordejon, J. Taylor and K. Stokbro, *Phys. Rev. B*, 2002, **65**, 165401-17.

[30] Y. Xue, S. Datta and M. A. Ratner, *J. Chem. Phys.*, 2001, **115**, 4292-4299.

[31] W. Su, J. Jiang, W. Lu and Y. Luo, *Nano Lett.*, 2006, **6**, 2091-2094.

[32] G. C. Solomon, C. Herrmann, T. Hansen, V. Mujica and M. A. Ratner, *Nat. Chem.*, 2010, **2**, 223-228.

[33] GAUSSIAN09, revision A.1, Gaussian, Inc., Wallingford, CT, 2009.

[34] N. Sai, M. Zwolak, G. Vignale, M. Di Ventra, *Phys. Rev. Lett.*, 2005, **94**, 186810-4.

[35] E. Runge and E. K. U. Gross, *Phys. Rev. Lett.*, 1984, **52**, 997-1000.

[36] H. Song *et al.*, *Nature*, 2009, **462**, 1039-1043.

[37] S. Datta, *Electron Transport in Mesoscopic Systems* (Cambridge University Press: Cambridge, UK, 1997).

[38] M. Di Ventra, *Electrical Transport in Nanoscale Systems* (Cambridge: New York, 2008).

[39] C. Herrmann, G. C. Solomon and M. A. Ratner, *J. Am. Chem. Soc.*, 2010, **132**, 3682-3684.

[40] R. Pati, L. Senapati, P. M. Ajayan and S. K. Nayak, *Phys. Rev. B*, 2003, **68**, 1004071-4(R).

[41] A. R. Rocha *et al.*, *Nature Mater.*, 2005, **4**, 335-339.

[42] Z. Ning, Y. Zhu, J. Wang and H. Guo, *Phys. Rev. Lett.*, 2008, **100**, 056803-4.

[43] M. Zwolak and M. Di Ventra, *App. Phys. Lett.*, 2002, **81**, 925-927.

[44] H. Dalgleish and G. Kirczenow, *Phys. Rev. B*, 2005, **72**, 184407-5.

[45] K. H. Khoo, M. S. C. Mozzoni and S. G. Louie, *Phys. Rev. B*, 2004, **69**, 201401(R).

[46] C-W. Chen, M-H Lee and S. J. Clark, *Nanotechnology*, 2004, **15**, 1837-1843.

[47] J. Kong *et al.*, *Phys. Rev. Lett.*, 2001, **87**, 106801-4.

[48] B. Xu, X. Xiao, X. Yang, L. Zang and N. Tao, *J. Am. Chem. Soc.*, 2004, **127**, 2386-2387.

[49] M. Cinchetti *et al.*, *Natur Mater.*, 2009, **8**, 115-119.

[50] M. Pati, M. McClain and A. Bandyopadhyay, *Phys. Rev. Lett.*, 2008, **100**, 246801-4.

	Dipole moment(a.u)			Polarizability(a.u)					
comp.	α^x	α^y	α^z	β^{xx}	β^{yx}	β^{yy}	β^{zx}	β^{zy}	β^{zz}
PC	0.079	0.143	9.594	692.78	-006.03	692.53	042.62	-000.72	5215.20
APC	0.952	0.788	8.578	677.26	-006.17	675.82	-022.72	122.57	5898.05

TABLE I: **Dipole moment & Polarizability.** Components of dipole moment (α) and polarizability (β) for parallel spin configuration (PC) and anti-parallel spin configuration (APC).

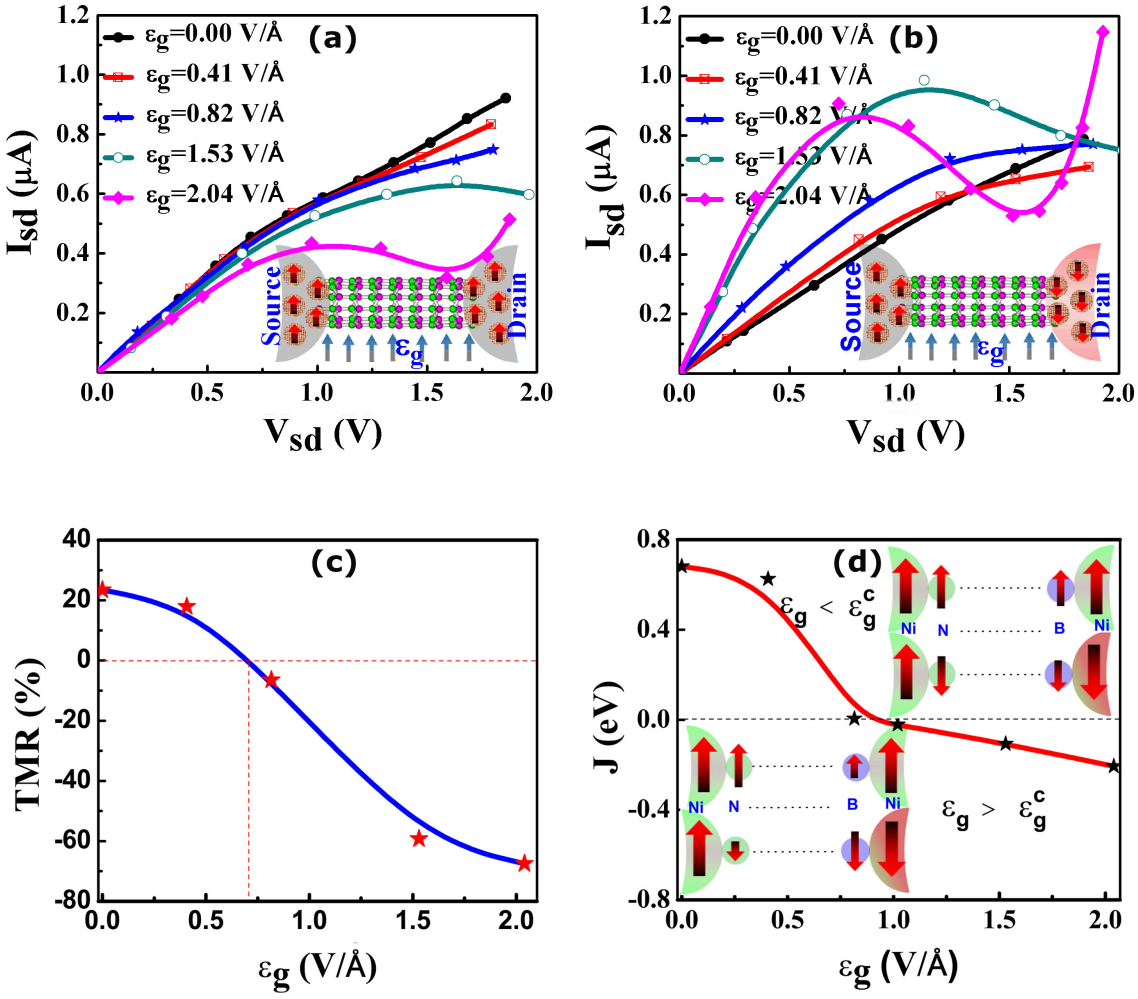

FIG. 1: **Switching in sign of TMR and J with transverse electric field.** I_{sd}-V_{sd} curves in a BNTQD tunnel junction for (a) PC and (b) APC as a function of ε_g. Insets show the schematic junction structures. (c) TMR vs. ε_g at V_{sd} of 0.2 V. (d) Exchange coupling (**J**) as function of ε_g. Inset shows the ε_g dependent spin-profiles at the interfaces. The height and width of the arrow determine the magnitude of magnetic moment. Up and down arrows denote positive and negative magnetic moments respectively.

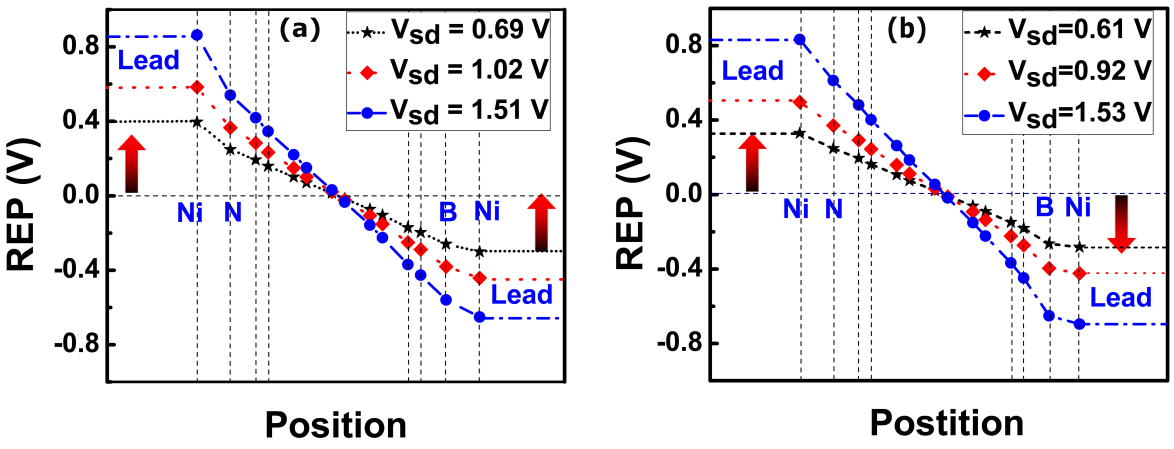

FIG. 2: **Bias dependent planar average electrostatic potential profile in BNTQD-Ni junction at different atomic positions.** (a) for PC and (b) for APC. The vertical dotted lines represent the planar atomic position of the device along the direction of current; the horizontal dotted line refers to the equilibrium situation; REP refers to the potential drop with respect to the equilibrium.

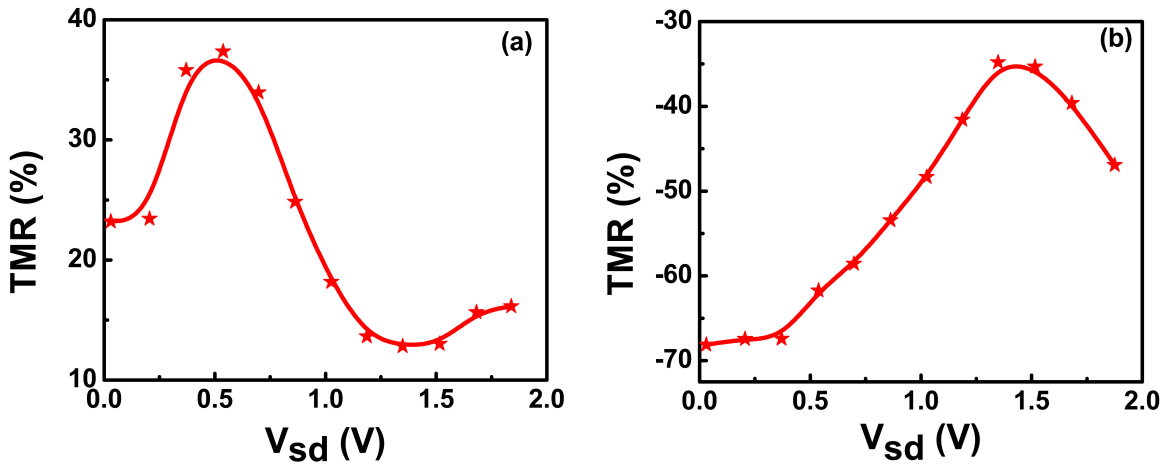

FIG. 3: **Bias dependent tunnel magnetoresistance (TMR).** TMR as a function of applied bias (V_{sd}) for (a) $\varepsilon_g = 0.00$ V/Å, and (b) $\varepsilon_g = 2.04$ V/Å.

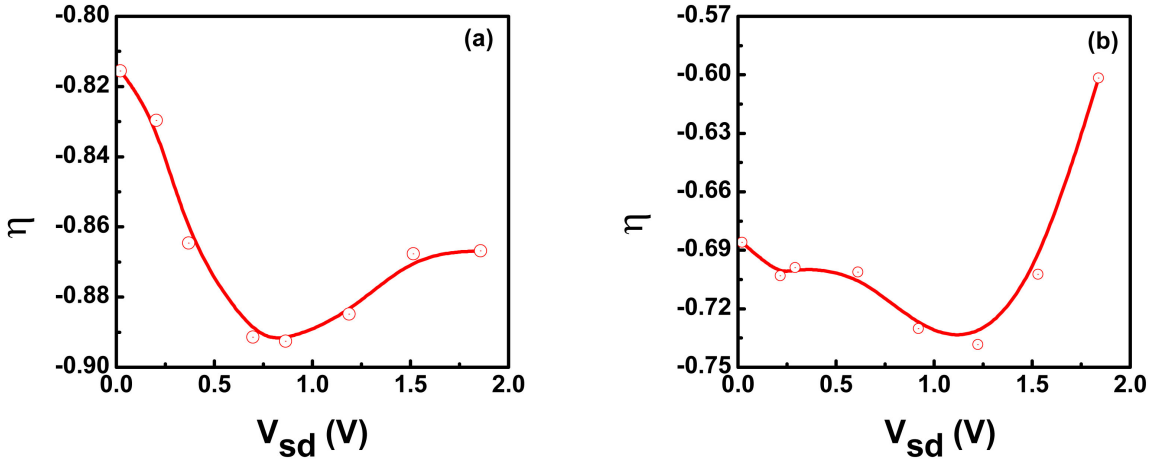

FIG. 4: **Bias dependent spin injection factor (η) in the BNTQD-Ni tunnel junction for ε_g = 0 V/Å.** (a) parallel spin configuration (PC), (b) anti-parallel spin configuration (APC). Since $I_{down} > I_{up}$, the η is found to be negative.

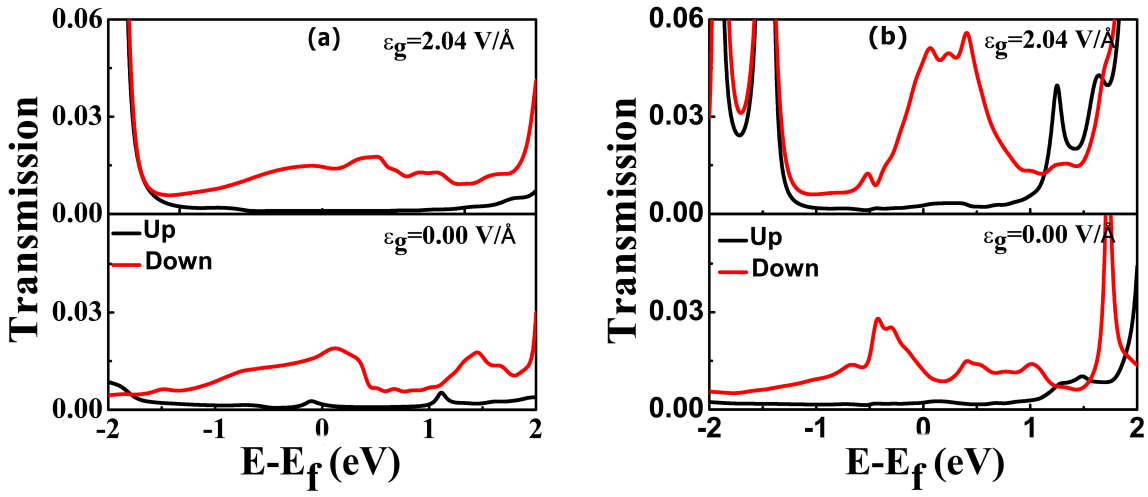

FIG. 5: **Transmission function.** ε_g dependent spin-polarized transmission for (a) parallel spin configuration and (b) anti-parallel spin configurations at V_{sd} of $\sim$ 0.2 V.

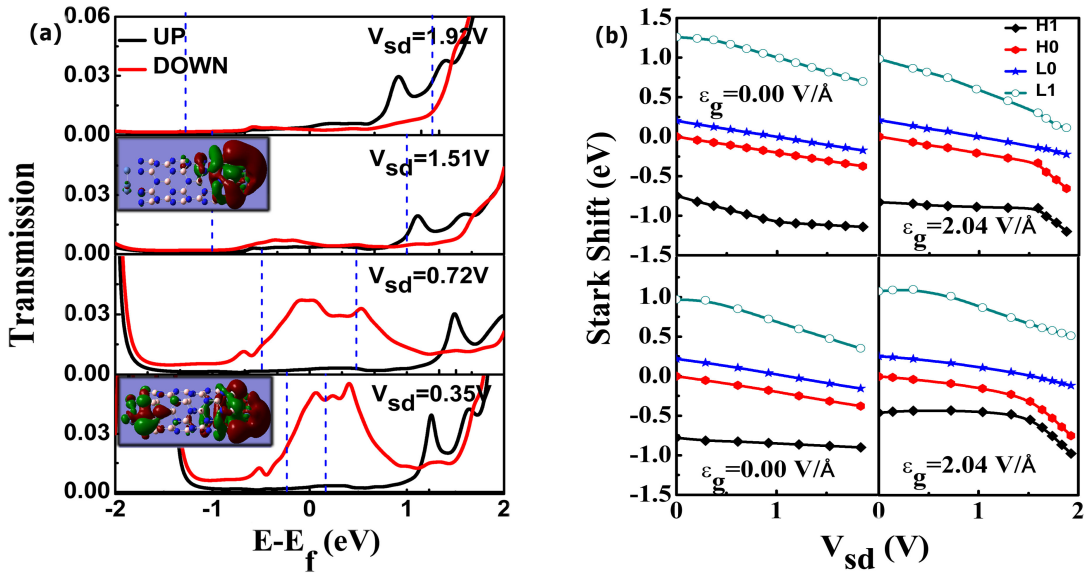

FIG. 6: **Stark effect.**(a) Bias dependent spin-polarized transmission for the APC of the extended system at $\varepsilon_g = 2.04$ V/Å. Dotted lines represent the chemical potential window (CPW). The inset shows the bias dependent spin-down HOMO for the APC at $\varepsilon_g = 2.04$ V/Å. (b) Bias dependent Stark shift corresponding to the frontier spin-down orbitals as a function of ε_g. Upper two panels are for PC and lower two panels are for APC. H0, H1 refer to the HOMO and HOMO-1, and L0, L1 refer to the LUMO and LUMO+1 spin-down orbitals in the extended system.